Article

# Halide Mixing and Phase Segregation in Cs$_2$AgBiX$_6$ (X = Cl, Br, and I) Double Perovskites from Cesium-133 Solid-State NMR and Optical Spectroscopy

Dominik J. Kubicki,[∇] Marcin Saski,[∇] Stuart MacPherson, Krzysztof Gałkowski, Janusz Lewiński,*
Daniel Prochowicz,* Jeremy J. Titman,* and Samuel D. Stranks*

Read Online
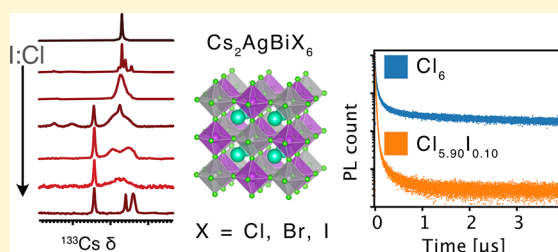
ACCESS | Metrics & More | Article Recommendations | SI Supporting Information

**ABSTRACT:** All-inorganic double perovskites (elpasolites) are a promising potential alternatives to lead halide perovskites in optoelectronic applications. Although halide mixing is a well-established strategy for band gap tuning, little is known about halide mixing and phase segregation phenomena in double perovskites. Here, we synthesize a wide range of single- and mixed-halide Cs$_2$AgBiX$_6$ (X = Cl, Br, and I) double perovskites using mechanosynthesis and probe their atomic-level microstructure using $^{133}$Cs solid-state MAS NMR. We show that mixed Cl/Br materials form pure phases for any Cl/Br ratio while Cl/I and Br/I mixing is only possible within a narrow range of halide ratios (<3 mol % I) and leads to a complex mixture of products for higher ratios. We characterize the optical properties of the resulting materials and show that halide mixing does not lead to an appreciable tunability of the PL emission. We find that iodide incorporation is particularly pernicious in that it quenches the PL emission intensity and radiative charge carrier lifetimes for iodide ratios as low as 0.3 mol %. Our study shows that solid-state NMR, in conjunction with optical spectroscopies, provides a comprehensive understanding of the structure−activity relationships, halide mixing, and phase segregation phenomena in Cs$_2$AgBiX$_6$ (X = Cl, Br, and I) double perovskites.

## INTRODUCTION

Since the first report of a lead halide perovskite solar cell (PSC) by Kojima et al. in 2009,[1] the field has quickly developed, leading to efficiencies above 25%.[2,3] Halide perovskites can be represented as ABX$_3$, where $A$ is a small cation such as methylammonium (CH$_3$NH$_3^+$, MA), dimethylammonium ((CH$_3$)$_2$NH$^+$, DMA), formamidinium (CH$_3$(NH$_2$)$_2^+$, FA), or cesium. The inorganic framework consists of [BX$_6$]$^{4−}$ octahedra, where $B$ is a divalent metal such as Pb$^{2+}$, while $X$ is a halide: I$^−$, Br$^−$, or Cl$^−$. One of the key concerns regarding lead halide PSCs is the environmental toxicity of water-soluble lead.[4] This problem has been addressed by a partial or complete replacement of lead in the perovskite structure by other cations such as Sn$^{2+}$ and Ge$^{2+}$.[5–8] The 3D perovskite structure can also be preserved using a mixture of mono- and trivalent cations such as Ag$^+$ and In$^{3+}$ or Bi$^{3+}$, Tl$^{3+}$,[9] leading to the double perovskite (elpasolite) structure.[10–13] Lower dimensionality structures based on Bi$^{3+}$, Sb$^{3+}$, and Cu$^{2+}$ and featuring suitable band gaps have been introduced; however, the reported power conversion efficiencies of solar cells typically do not exceed 1%.[6,14,15] While tin(II)- and germanium(II)-based perovskites are unstable in ambient conditions due to their propensity to oxidize and disproportionate, the recently discovered Ag/In and Ag/Bi elpasolites have exceptionally high ambient stability. After the first report on the synthesis of Cs$_2$AgBiBr$_6$ and

Cs$_2$AgBiCl$_6$,[16,17] the Br-based material has been shown to form high-quality thin films suitable for the fabrication of solar cells with power conversion efficiencies reaching 1, 4, and 2.5% using vacuum deposition and solution processing, respectively.[18–20] The material has been further investigated computationally,[18,21] as a single crystal,[22,23] and its band gap has been shown to be tunable by alloying with Pb$^{2+}$,[24] Sn$^{2+/4+}$,[25] Tl$^{3+}$,[9] In$^{3+}$, and Sb$^{3+}$.[13] Very recently, mixed-halides Cs$_2$AgBiCl$_{6−x}$Br$_x$ have been investigated both theoretically[26,27] and experimentally.[27,28] However, very little is known about halide miscibility and phase segregation phenomena in this class of materials. For example, optical properties have been previously calculated for Cs$_2$AgInX$_6$ (X = Cl, Br, and I) double perovskites, assuming that halides can be mixed in any ratio, leading to pure-phase materials.[12] In general, however, phase segregation is expected to occur for some halide combinations due to differences in ionic radii.[29]

Solid-state magic angle spinning (MAS) NMR has been established as the primary tool for studying the atomic-level microstructure of hybrid halide perovskites.[30] We and other groups have shown its use for determining local changes induced by composition engineering: A/B-site cation[31−39] and halide[29,40−44] mixing and phase segregation as well as surface interactions between perovskites and organic passivation dopants.[45−48] Solid-state NMR has also been used to study the degradation of hybrid halide perovskites[49] and the dynamics of their constituents: A-site cation reorientation[31,50−53] and ion diffusion.[54−56] Many of these solid-state NMR studies used cesium NMR as one of the local probes owing to the importance of cesium in this class of materials as well as the advantageous NMR properties of cesium—high sensitivity and spectral resolution. Cesium-133 is a 100% abundant spin-7/2 characterized by a receptivity of about 280 times higher than that of $^{13}$C. Its small quadrupole moment ($-0.343$ fm$^2$) means that, in practice, it can be manipulated like a spin-1/2 nucleus.[57] The $^{133}$Cs shift range spans about 400 pm, which translates to wide shift dispersion and therefore high spectral resolution. In the case of halide perovskites, cesium NMR studies have allowed discernment between cesium-containing phases with different dimensionalities,[32,44] different halide compositions,[39,44,58] and different nearest neighbor A-site compositions.[32] Cesium NMR has been widely used to study cesium-containing inorganic[59−64] and organic[65] materials.

Mechanosynthesis is a facile solid-state protocol for preparing various complex materials without the use of solvents. It is an attractive alternative to wet chemistry methods as it allows for shorter reaction times, facilitates product processing, and alleviates solubility restrictions.[66,67] We have previously developed mechanosynthesis of hybrid[68−70] and all-inorganic[32] halide perovskites and have shown using solid-state MAS NMR and X-ray diffraction (XRD) that it leads to materials indistinguishable from those prepared using solution-processed thin films.[32,34] The key advantage of mechanosynthesis is that it makes it possible to prepare large quantities of materials, allowing for NMR data acquisition with high sensitivity.

Here, we synthesize a wide range of single- and mixed-halide Cs$_2$AgBiX$_6$ (X = Cl, Br, and I) double perovskites using mechanosynthesis and establish their full binary phase diagrams using $^{133}$Cs solid-state MAS NMR and XRD, which probe the local and long-range structures, respectively (Figure 1). We show that mixed Cl/Br materials form pure phases for any Cl/Br ratio, while Cl/I and Br/I mixing is only possible within a narrow range of halide ratios and leads to complex mixtures of products for other ratios. We characterize the optical properties of the resulting materials and show that halide mixing does not lead to substantial tunability of the PL emission. We find that iodide doping is particularly pernicious in that it quenches the PL emission intensity and radiative charge carrier lifetimes for iodide ratios as low as 0.3 mol %.



**Figure 1.** Schematic representation of the crystal structure of Cs$_2$AgBiX$_6$ (X = Cl, Br, and I) double perovskites investigated in this work.

previously for lead halide perovskites.[68,69] The precursors were stored under argon. The materials were synthesized by grinding the reactants in an electric ball mill (Retsch MM − 400) using a Teflon grinding jar (10 mL) and ball (∅10 mm) for 30 min at 30 Hz. The quantities of reagents used in the synthesis are given in the Supporting Information.

**NMR Measurements.** Solid-state MAS NMR spectra of $^{133}$Cs (39.3 MHz) were recorded on a Chemagnetics 7.0 T spectrometer equipped with a 4.0 mm PENCIL MAS probe using a Bloch decay (30° − acquire) with 50 kHz RF strength and a recycle delay of 30 s. Pulse lengths were calibrated on Cs$_2$AgBiCl$_6$ and correspond to solution pulse lengths owing to the absence of substantial second-order quadrupolar effects for $^{133}$Cs; 16−64 scans were acquired. The spectra were fitted using a linear combination of Lorentzian and Gaussian curves (Voigt profile) using MestReNova 14.1.0 (Mestrelab Research). For very broad signals, the lowest feasible number of components was used to satisfactorily represent the line shape without overfitting. The numerical values are reported in Table S1. We also recorded quantitative $^{133}$Cs spectra for selected samples and found no qualitative differences with respect to those recorded using a shorter recycling delay (Figures S8−S10, Table S2).

**X-ray Diffraction.** Diffractograms were recorded on an X'Pert MPD PRO (Panalytical) diffractometer equipped with a ceramic tube (Cu anode, λ = 1.54060 Å), a secondary graphite (002) monochromator, and an RTMS X'Celerator (Panalytical) in an angle range of 2θ = 10 to 50°, by step scanning with a step of 0.02 degree.

**Photoluminescence Measurements.** Steady-state photoluminescence spectra were acquired with a Maya2000 Pro spectrometer. Excitation was provided by a 405 nm continuous-wave laser source with an incident irradiance of ∼100 mW/cm$^2$.

**Photoluminescence Quantum Efficiency (PLQE).** PLQE measurements were conducted to establish the ratio of radiative decay to nonradiative decay in photoexcited samples. Excitation was provided by a continuous-wave diode laser (Thorlabs L405P20, 3.06 eV photon energy) at a solar equivalent intensity of ∼100 mW/cm$^2$ (200 μW incident power, 510 μm effective beam diameter). Following the method set out by De Mello et al., three measurements were made on each sample to establish the external PLQE.[71] The samples were housed in an integrating sphere to collect all PL and any reflected or transmitted laser light, which was then fiber-coupled to a spectrometer (Andor iDus DU420A-BVF). Measurements were recorded with the laser directly on the sample, off the sample (i.e., with the beam aimed at the inner wall of the integrating sphere), and with no sample present in the integrating sphere.

**Time-Correlated Single-Photon Counting Measurements.** Time-resolved photoluminescence measurements were carried out using a confocal microscope setup (PicoQuant, MicroTime 200). A 405 nm pulsed diode laser (PDL 828 "SEPIA II", PicoQuant, pulse width ∼100 ps) was focused onto the surface of the microcrystalline

## EXPERIMENTAL SECTION

**Materials.** The following materials were used: CsI (Tokyo Chemical Industry (TCI), >99.0%), CsBr (TCI, >99.0%), CsCl (TCI, >99.0%), AgI (ABCR, 99.9%), AgBr (ABCR, 99,9%), AgCl (ABCR, 99.9%), BiI$_3$ (Sigma-Aldrich, 99.998%), BiBr$_3$ (ABCR, 99.0%), and BiCl$_3$ (ABCR, 99.9%).

**Perovskite Mechanosynthesis.** The double perovskites were prepared using mechanosynthesis following methods reported
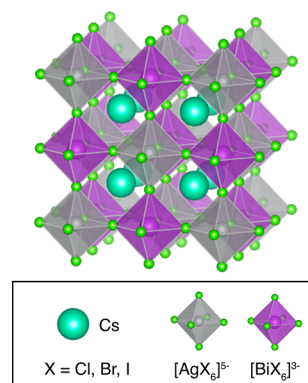
powder sandwiched between two glass coverslips using an air objective (20 ×, 0.4 NA). The emission signal was separated from the excitation light using a dichroic mirror (Z405RDC, Chroma). Repetition rates of 0.2 MHz were used with an average energy density of 2.5 $\mu J/cm^2$. Photoluminescence photon arrival times were binned in 400 ps intervals.

## ■ RESULTS AND DISCUSSION

**Mechanosynthesis of Mixed-Halide $Cs_2AgBiX_6$ (X = Cl, Br, and I) Double Perovskites.** We prepared a series of single- and mixed-halide $Cs_2AgBiX_6$ (X = Cl, Br, and I) double perovskite materials using mechanosynthesis, in analogy to the protocols previously developed for lead halide perovskites.[67,72] Examination of the resulting powders by powder X-ray diffraction shows the formation of $Cs_2AgBiBr_6$, $Cs_2AgBiCl_6$, and mixed-halide $Cs_2AgBiCl_{6-x}Br_x$ double perovskites for any ratio of halides, as indicated by a linear shift of the diffraction peaks on going from the pure-chloride to the pure-bromide materials (Figure S1), in full agreement with a recent study by Gray et al.[28,73] On the other hand, the XRD patterns of the materials formally corresponding to $Cs_2AgBiCl_{6-x}I_x$ and $Cs_2AgBiBr_{6-x}I_x$ show peaks attributable to phase-pure double perovskites only for low iodide doping levels and a complex mixture of products for higher iodide contents (Figures S2 and S3). In order to corroborate and refine the long-range picture provided by XRD, we employ solid-state NMR and investigate the local structure, as probed by the $^{133}Cs$ nuclei in the materials.

**Chloride-Bromide Mixing in $Cs_2AgBiX_6$ (X = Cl and Br).** Figure 2 shows $^{133}Cs$ solid-state MAS NMR spectra of
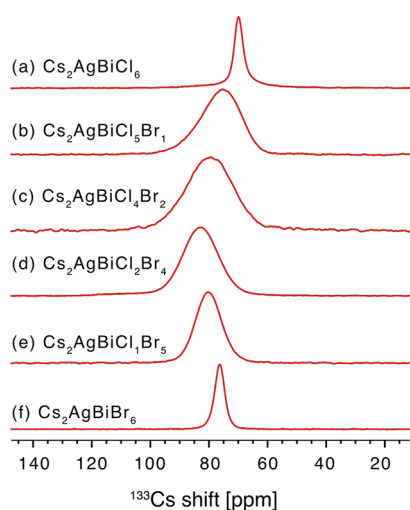


**Figure 2.** $^{133}Cs$ solid-state MAS NMR spectra of mixed-halide $Cs_2AgBiCl_{6-x}Br_x$ compositions at 7.0 T, 12 kHz MAS and 298 K: (a) x = 0, (b) x = 1, (c) x = 2, (d) x = 4, (e) x = 5, (f) x = 6.

bulk mechanochemical $Cs_2AgBiCl_{6-x}Br_x$ (x = 0−6) double perovskites. The spectra of both $Cs_2AgBiCl_6$ (δ = 69.9 ppm) and $Cs_2AgBiBr_6$ (δ = 76.3 ppm) contain a single peak, consistent with the presence of a single cesium site in the crystal structure of these materials. The spectra of the mixed bromide/chloride compositions are considerably broader (see Figure S8 and Table S1 for the fitted fwhm values), which we attribute to the presence of halide disorder. The $Cs^+$ sites in double perovskites have a dodecahedral coordination environment, that is, 12 halide nearest neighbors. In the mixed-halide compositions, these 12 sites are occupied by a varying ratio of

Cl and Br anions, which in turn leads to the presence of a distribution of cesium environments with slightly differing $^{133}Cs$ shifts. Halides which are farther away may also contribute to the chemical shift of the cesium site through long-range effects. Figures S12−14 and Table S3 show the calculated random distribution of nearest-neighbor halide environments for the experimental Cl-to-Br ratios studied here and for radii of 5, 10, and 15 Å around the cesium site, which correspond to 12, 60, and 240 nearest halide neighbors, respectively. Both the experimental spectra and the calculated random distributions of environments are Gaussian, which shows that the halides are distributed randomly in the mixed chloride-bromides; that is, there is no halide clustering. This result is in perfect agreement with a recent computational study of $Cs_2AgBiCl_{6-x}Br_x$ double perovskites.[28] We note that the $^{133}Cs$ shift is not a linear function of the Cl/Br ratio (Figure S4). Similar nonlinearity caused by the nonadditive effect of the nearest and next-nearest neighbors on the chemical shift has been previously observed for $^{89}Y$ and $^{119}Sn$ in solid solutions of mixed-metal pyrochlores and for $^{13}C$ in mixed-halide hybrid tin(II) halide perovskites.[74−76] We also note that the broadening and signal positions are not field-dependent, which confirms that they are caused by chemical disorders rather than quadrupolar effects (Figure S8c). No other cesium-containing phases were detected in this group of materials (see Figure S7 for the full range spectra). The XRD data corroborate that the materials are phase pure and show a linear shift of all diffraction peaks as a function of the Cl:Br ratio (Figure S1). Similarly, the band gaps obtained from absorption spectra are a linear function of the Cl:Br ratio (Figures S17 and S18). We, therefore, conclude that $Cs_2AgBiCl_6$ and $Cs_2AgBiBr_6$ are miscible in any proportion and form solid solutions for any Cl/Br ratio.

**Bromide−Iodide Mixing in $Cs_2AgBiX_6$ (X = Br and I).** Figure 3 shows $^{133}Cs$ solid-state MAS NMR spectra of bulk mechanochemical $Cs_2AgBiBr_{6-x}I_x$ (x = 0−6) double perovskites and related cesium-containing nonperovskite phases. While the spectrum of $Cs_2AgBiBr_6$ is best fitted with a single component (Figure 3a), the addition of iodide ions leads to the appearance of a small second component at higher shift values whose intensity relative to the main perovskite peak increases as the I-to-Br mole ratio increases from 0.02:5.98 to 0.20:5.80 (Figure 3b−d). This new component corresponds to cesium environments with one or more iodide nearest neighbors. In practice, the substantially populated (>1%) combinations are those with 1 (for I/Br = 0.02:5.98 and 0.10:5.90) and 2 (for I/Br = 0.20:5.80) iodides surrounding the dodecahedral cavity (Figure S15 and Table S4). This is accompanied by slight changes in the shift and line width of the initial component corresponding to only-bromide $[AgBr_6][BiBr_6]^{4-}$ nearest neighbors (76.3 ppm and 145 Hz in $Cs_2AgBiBr_6$ and 75.7 and 178 ppm in $Cs_2AgBiBr_{5.90}I_{0.10}$; see Figure S9 and Table S1 for the fitted values). These more subtle changes are likely due to the long-range effect of iodide substitution, i.e., outside the first dodecahedral coordination environment, on cesium sites which only have bromides in their first coordination sphere.

As the I/Br ratio increases further (Figure 3e), new cesium environments appear in the 38−71 ppm and 87−110 ppm ranges, which we assign to mixed-halide nonperovskite $Cs_3Bi_2I_{9-x}Br_x$ and $Cs_3Bi_2Br_{6-x}I_x$ phases, respectively. The onset of phase segregation is also clearly visible in the 110−350 ppm range, where a number of nonperovskite phases become apparent for I/Br ratios greater than 0.20:5.80. These phases do not match any of the reference phases, and we did
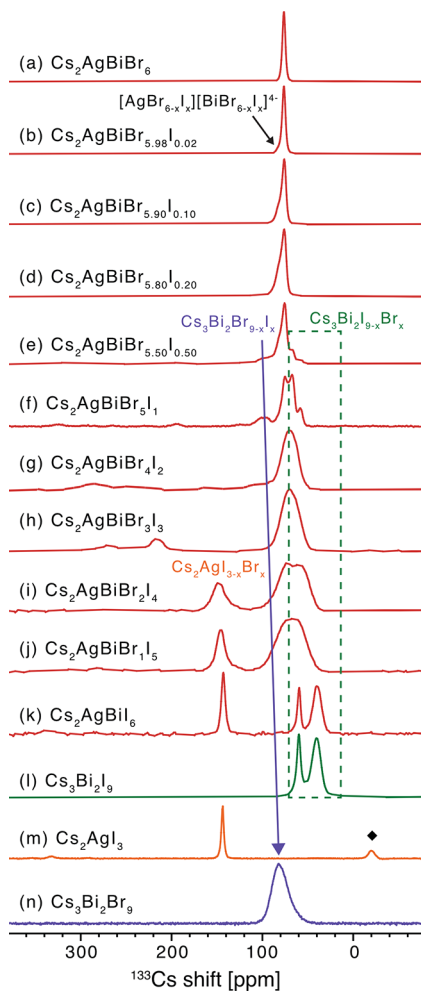
**Figure 3.** $^{133}$Cs solid-state MAS NMR spectra of (a−k) mixed-halide Cs$_2$AgBiBr$_{6−x}$I$_x$ compositions and (l−n) related nonperovskite phases at 7.0 T, 12 kHz MAS and 298 K: (a) x = 0, (b) x = 0.02, (c) x = 0.10, (d) x = 0.2, (e) x = 0.5, (f) x = 1, (g) x = 2, (h) x = 3, (i) x = 4, (j) x = 5, (k) x = 6, (l) Cs$_3$Bi$_2$I$_9$, (m) Cs$_2$AgI$_3$, and (n) Cs$_3$Bi$_2$Br$_9$. The black diamond indicates an impurity phase (likely CsAg$_2$I$_3$).
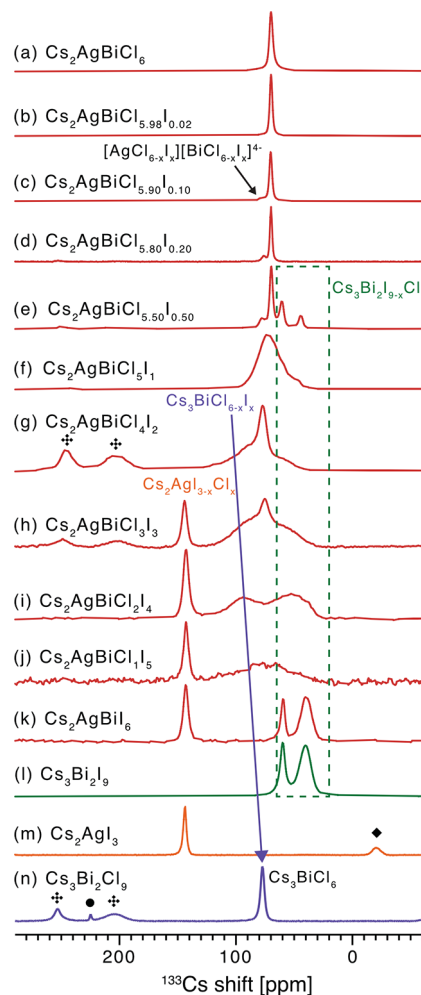
**Figure 4.** $^{133}$Cs solid-state MAS NMR spectra of mixed-halide Cs$_2$AgBiCl$_{6−x}$I$_x$ compositions (a−k) and related nonperovskite phases (l−n) at 7.0 T, 12 kHz MAS and 298 K: (a) x = 0, (b) x = 0.02, (c) x = 0.10, (d) x = 0.2, (e) x = 0.5, (f) x = 1, (g) x = 2, (h) x = 3, (i) x = 4, (j) x = 5, (k) x = 6, (l) Cs$_3$Bi$_2$I$_9$, (m) Cs$_2$AgI$_3$, (n) Cs$_3$Bi$_2$Cl$_9$. The black diamond indicates an impurity phase (likely CsAg$_2$I$_3$). The heavy four balloon-spoked asterisk indicates unknown nonperovskite impurity phases. The black circle indicates CsCl.

not attempt to identify them. Finally, the composition formally corresponding to Cs$_2$AgBiI$_6$ (Figure 2k) is a mixture of two nonperovskite phases: Cs$_3$Bi$_2$I$_9$ (Figure 2l) and Cs$_2$AgI$_3$ (Figure 2m). This result is consistent with previous reports which identified that the double perovskite phase of Cs$_2$AgBiI$_6$ does not form,[77] although the synthesis of its nanocrystalline form has been reported.[78] We note that the spectrum of Cs$_3$Bi$_2$I$_9$ has two peaks that correspond to two inequivalent cesium sites in the asymmetric unit cell, consistent with a previous report.[79] The XRD data corroborate these assignments and display the same phase segregation phenomena, although their diffraction fingerprint is considerably more complex (Figure S2). Taken together, these results show that small amounts of iodide can replace Br in the Cs$_2$AgBiBr$_6$ structure, but phase segregation occurs for I/Br ratios higher than 0.20:5.80 (3 mol % I). This conclusion can also be expressed in terms of the nearest neighbor count: phase segregation occurs for stoichiometries, which would lead to a substantial (>1%) population of cesium sites with more than two nearest neighbor iodide ions.

**Chloride-Iodide Mixing in Cs$_2$AgBiX$_6$ (X = Cl, I).** Figure 4 shows $^{133}$Cs solid-state MAS NMR spectra of bulk

mechanochemical Cs$_2$AgBiCl$_{6−x}$I$_x$ (x = 0−6) double perovskites and related cesium-containing nonperovskite phases. The replacement of a small amount of chloride, ongoing from Cs$_2$AgBiCl$_6$ (δ = 69.9 ppm, Figure 4a) to Cs$_2$AgBiCl$_{5.98}$I$_{0.02}$ (δ = 69.9 ppm, Figure 4b), does not lead to an appreciable change in the spectrum. However, for I/Cl = 0.10:5.90 (Figure 4c), a new chemical environment appears at δ = 78.2 ppm, which likely corresponds to new [AgCl$_{6−x}$I$_x$][BiCl$_{6−x}$I$_x$]$^{4−}$ environments in which the cesium site has at least one iodide in its first coordination sphere (see Figure S10 and Table S1 for the fitted values). As the I/Cl ratio increases, the relative contribution of this new environment increases from 10 to 14% (ascertained from the fitted peak area), for I/Cl ratios of 0.10:5.90 and 0.20:5.80, respectively. The relative contribution of this signal does not increase beyond this I/Cl ratio. Instead, as the I/Cl ratio increases further, new signals appear at 44.3 and 60.6 ppm, which we assign to a mixed-halide non-perovskite Cs$_3$Bi$_2$I$_{9−x}$Cl$_x$ phase (Figure 4e). The narrow component corresponding to native [AgCl$_6$][BiCl$_6$]$^{4−}$ environments disappears at I/Cl = 1:5 where only a single broad
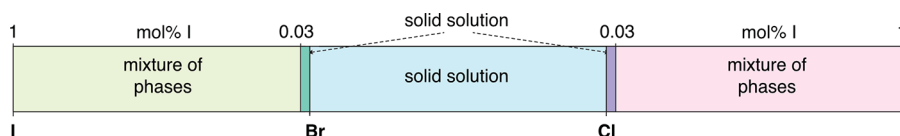
**Figure 5.** Schematic representation of the $Cs_2AgBiX_6$ (X = Cl/Br, Br/I and Cl/I) miscibility diagram established in the present work based on [133]Cs MAS NMR data.

convoluted signal is visible. For I/Cl ≥ 2:4, a new species appears, which we assign to a mixed-halide nonperovskite $Cs_3BiCl_{6-x}I_x$ phase (Figure 4g−j). The broadened 3D double mixed-halide perovskite signal is distinguishable for ratios of I/Cl = 2:4 and 3:3 (at $\delta$ = 76.9 and 75.1 ppm, respectively), but it disappears for I/Cl ≥ 4:2 at which point only nonperovskite phases are present. The larger line width of the double perovskite peak for I/Cl = 2:4 (fwhm = 261 Hz) as compared to I/Cl = 0.20:5.80 (fwhm = 159 Hz) is due to an increase in the halide disorder around the cesium site. This result shows that iodides can, in principle, be incorporated in ratios slightly higher than I/Cl = 0.20:5.80, although, in all experiments, this is accompanied by the formation of nonperovskite phases that exist in equilibrium with the perovskite phase. In addition, for high I/Cl ratios (I/Cl ≥ 3:3), a silver-rich mixed-halide $Cs_2AgI_{3-x}Cl_x$ phase ($\delta$ = 143−144 ppm) becomes apparent. Therefore, analogous to the Br/I case discussed above, phase segregation occurs in materials in which the nominal I/Cl ratio would lead to the nearest neighbor count of iodide ions on a cesium site that is higher than 2 (Figure S16 and Table S5). The XRD data are in agreement with this interpretation and show clear segregation into a complex mixture of phases for I/Cl > 0.50:5:50 (Figure S3). We conclude that chloride ions can replace iodide ions in the structure of $Cs_2AgBiCl_6$ to form phase-pure materials up to I/Cl ratios of 0.20:5.80, while phase segregation of nonperovskite phases occurs above this ratio.

We summarize the above findings on a phase diagram which shows the miscibility range for the three types of two-halide mixtures investigated here: full miscibility in any ratio for Br/Cl and very limited miscibility for the Br/I and Cl/I compositions (Figure 5). It is interesting to note that the diagram is symmetrical; that is, both $Cs_2AgBiCl_6$ and $Cs_2AgBiBr_6$ can only accommodate up to 3 mol % iodide through halide substitution, corresponding to no nearest-neighbor iodides in the lattice. This behavior is different compared to lead halide perovskites, where full Br/Cl and Br/I halide miscibility has been reported for CsPbX$_3$,[44] MAPbX$_3$,[29,40,41] and FAPbX$_3$[43] (X = Br/Cl and Br/I) while no I/Cl miscibility was observed for MAPbX$_3$ (X = Br/Cl and Br/I).[29]

**Optoelectronic Properties of Mixed-Halide $Cs_2AgBiX_6$ (X = Cl, Br, and I) Phases.** We now evaluate the effect halide mixing has on the optoelectronic properties of cesium silver−bismuth double perovskites. Figure 6 shows the PL spectra of the representative bulk mechanochemical compositions. $Cs_2AgBiCl_6$ is the most emissive out of the samples measured here (PLQE of 0.76%), consistent with previous reports (Figure 6a, blue).[80] Its spectrum covers the range between 460 and 1000 nm with a broad fwhm of about 220 nm (we note that the emission is a skewed Gaussian, see Table S6). The broad emission peak has been previously attributed to self-trapped excitonic species.[81,82] $Cs_2AgBiBr_6$ prepared in an analogous way has an emission intensity which is ∼66 times lower than that of the pure chloride material and a similar broadband emission spectrum (Figure 6b, blue; Figure S19,
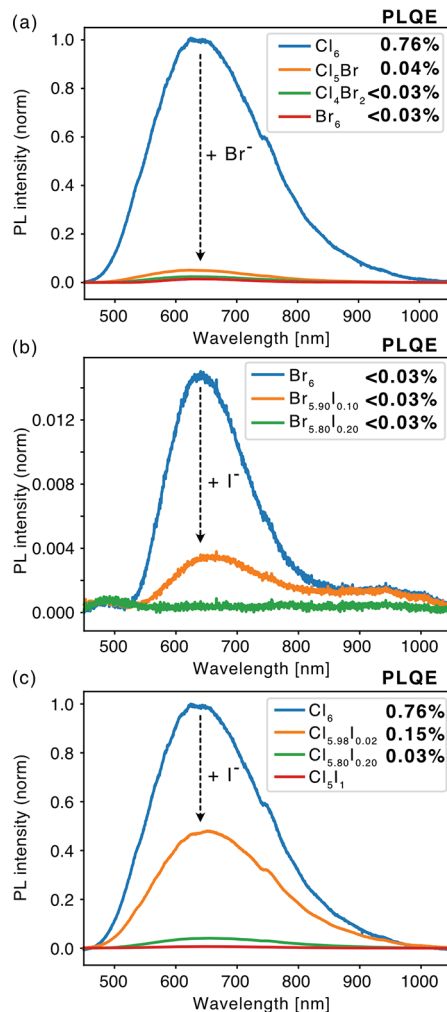


**Figure 6.** PL spectra and PLQE of bulk mechanochemical mixed-halide compositions (a) $Cs_2AgBiCl_{6-x}Br_x$ (x = 0, 1, 2, and 6), (b) $Cs_2AgBiBr_{6-x}I_x$ (x = 0, 0.10, and 0.20), and (c) $Cs_2AgBiCl_{6-x}I_x$ (x = 0, 0.02, 0.20, and 1). Excitation wavelength: 405 nm. The discontinuity at ∼720 nm is due to a fiber artefact. For conciseness, only the halide composition is given in the legend.

Table S6). Bromide substitution into $Cs_2AgBiCl_6$ leads to intermediate PL intensities: 19-fold and 41-fold reduction with respect to pure $Cs_2AgBiCl_6$ for Br:Cl ratios of 1:5 and 2:4, respectively (Figure 6a). The PLQE of the Br:Cl = 1:5 material is 0.04%, while for the other mixed-halide materials as well as pure bromide, it is below the threshold of reliable detection. Therefore, bromide-addition to $Cs_2AgBiCl_6$ leads to substantial photoluminescence quenching. Iodide addition to $Cs_2AgBiCl_6$ has a similar effect: the incorporation of iodide at the I/Br ratio of 0.10:5.90 (i.e., 1.7 mol % iodide) decreases the luminescence fivefold with respect to the pure-bromide material, while at the ratio of 0.20:5.80 (i.e., 3.3 mol % iodide), there is essentially no detectable luminescence (Figure

6b). Similarly, the PL quenching effect is very pronounced in iodide-doped chlorides: we observe a 2-fold, 24-fold, and 142-fold intensity decrease with respect to $Cs_2AgBiCl_6$ for I/Cl ratios of 0.02:5.98 (0.3 mol % I), 0.20:5.80 (3.3 mol % I), and 1:5 (10.6 mol % I), respectively (Figure 6c). The PLQE decreases from 0.76% for the pure chloride to 0.15% for $Cs_2AgBiCl_{5.98}I_{0.02}$ and 0.03% for $Cs_2AgBiCl_{5.80}I_{0.20}$. We note that the PL wavelength distribution and peak wavelength change only slightly as a function of the halide composition (see Figures S19−21 and Tables S6 and S7 for the normalized PL spectra and fitted values, respectively). This is expected for self-trapped exciton emission since it is the strong electron−phonon coupling that acts to broaden the transitions via scattering.[81,83] We, therefore, conclude that not only does halide mixing not lead to substantial PL emission tunability, but it also dramatically decreases the PL emission intensity.

Finally, we employ time-correlated single-photon counting (TCSPC) to evaluate the effect halide mixing has on the PL lifetimes. Figure 7 shows the TCSPC time traces for the three groups of mixed-halide materials (Cl/Br, Br/I, and Cl/I).

All the traces are nonlinear on a semilogarithmic scale, implying that the radiative recombination processes at play are more complicated than what can be modeled through a single exponential. Therefore, we do not fit the data to a physical model and limit ourselves to a qualitative description.[84] $Cs_2AgBiCl_6$ has a pronounced long-lived component, previously attributed to the intrinsic PL lifetime driven by self-trapped excitons in this class of compounds (Figure 7a).[17,85]

The contribution of the long-lived component decreases significantly in the mixed Cl/Br sample and is essentially absent in $Cs_2AgBiBr_6$. Iodide doping also reduces this long-lived component, and in this case, the quenching effect is considerably stronger than the pure halide cases, consistent with the PL intensities in Figure 6. While $Cs_2AgBiBr_6$ still exhibits an appreciable signal up to around 2 $\mu$s, the iodide-doped sample, $Cs_2AgBiBr_{5.90}I_{0.10}$, decays to negligible values within less than 0.2 $\mu$s (Figure 7b).

The quenching effect of iodide is evident when comparing $Cs_2AgBiCl_6$ and $Cs_2AgBiCl_{5.90}I_{0.10}$ — the presence of as little as 1.7 mol % $I^-$ leads to a complete quenching of the long-lived component (Figure 7c). While there is still some debate on the exact photophysical mechanism of recombination in halide double perovskites, it is accepted that (a) the long-lived component corresponds to the intrinsic recombination of the materials,[17] and (b) it is most likely caused by self-trapped excitons.[81,85] In summary, the TCSPC results show that both Br- and I- doping of $Cs_2AgBiCl_6$ lead to the quenching of the long-lived component associated with self-trapped excitons. We identify that the atomic-level mechanism of quenching is the incorporation of Br-/I- into the parent lattice of $Cs_2AgBiCl_6$, leading to a mixed-halide double perovskite.

## ◼ CONCLUSIONS

In conclusion, we have synthesized a broad range of mixed-halide $Cs_2AgBiX_6$ (X = Cl, Br, and I) double perovskites and employed solid-state $^{133}Cs$ MAS NMR to identify the limits of miscibility of the different halides. We have found that chlorides and bromides can be mixed in any ratio, leading to phase-pure double perovskites, while iodides can be incorporated into the bromide-only and chloride-only lattices only at low concentrations (<3 mol %). Higher iodide doping levels lead to a complex mixture of silver-rich and bismuth-rich nonperovskite phases. The mixed-halide materials exhibit a
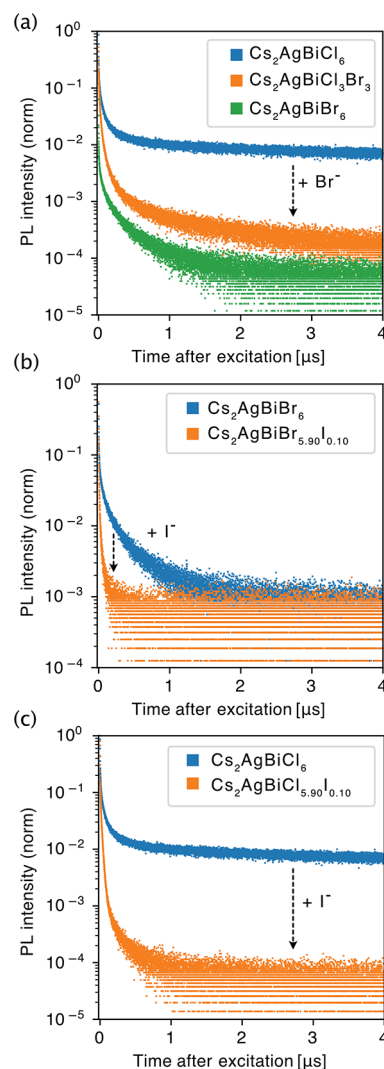


**Figure 7.** TCSPC time traces of bulk mechanochemical mixed-halide compositions (a) $Cs_2AgBiCl_{6-x}Br_x$ (x = 0, 3, and 6), (b) $Cs_2AgBiBr_{6-x}I_x$ (x = 0 and 0.10), (c) $Cs_2AgBiCl_{6-x}I_x$ (0 and 0.10). Excitation wavelength: 405 nm, repetition rate: 0.2 MHz, average energy density per pulse: 2.5 $\mu$J/$cm^2$.

very broad self-trapped excitonic PL emission (c.a. 460−1000 nm), which does not substantially depend on the halide composition. These results reveal that halide mixing is not a viable way of tuning the emission characteristics of bulk microcrystalline $Cs_2AgBiX_6$ (X = Cl, Br, and I) double perovskites. Notably, we have found that iodide doping of $Cs_2AgBiCl_6$ and $Cs_2AgBiBr_6$ leads to a dramatic decrease of the PL intensity and quenches the photophysical process responsible for the long-lived PL decay observed in the pure-chloride and pure-bromide materials, which we identify as being due to the incorporation of iodide into the perovskite lattice of these materials. We have therefore demonstrated that the use of optical spectroscopies in conjunction with atomic-level insight from solid-state NMR provides a comprehensive understanding of the structure−activity relationships, halide mixing, and phase segregation phenomena in $Cs_2AgBiX_6$ (X = Cl, Br, and I) double perovskites.

## ■ ASSOCIATED CONTENT

### ⓈI Supporting Information

The Supporting Information is available free of charge at https://pubs.acs.org/doi/10.1021/acs.chemmater.0c01255.

Synthesis of the materials; additional XRD; NMR data analysis; UV−Vis measurements; and PL measurements (PDF)

## ■ AUTHOR INFORMATION

### Corresponding Authors

**Janusz Lewiński** − *Institute of Physical Chemistry, Polish Academy of Sciences, Warsaw 01−224, Poland; Faculty of Chemistry, Warsaw University of Technology, Warsaw 00-664, Poland;* ⓘ orcid.org/0000-0002-3407-0395; Email: lewin@ ch.pw.edu.pl

**Daniel Prochowicz** − *Institute of Physical Chemistry, Polish Academy of Sciences, Warsaw 01−224, Poland;* ⓘ orcid.org/ 0000-0002-5003-5637; Email: dprochowicz@ichf.edu.pl

**Jeremy J. Titman** − *School of Chemistry, University of Nottingham, Nottingham NG7 2RD, U.K.;* Email: Jeremy.Titman@nottingham.ac.uk

**Samuel D. Stranks** − *Cavendish Laboratory, Department of Physics and Department of Chemical Engineering and Biotechnology, University of Cambridge, Cambridge CB3 0HE, U.K.;* ⓘ orcid.org/0000-0002-8303-7292; Email: sds65@ cam.ac.uk

### Authors

**Dominik J. Kubicki** − *Cavendish Laboratory, Department of Physics and Department of Chemical Engineering and Biotechnology, University of Cambridge, Cambridge CB3 0HE, U.K.;* ⓘ orcid.org/0000-0002-9231-6779

**Marcin Saski** − *Institute of Physical Chemistry, Polish Academy of Sciences, Warsaw 01−224, Poland*

**Stuart MacPherson** − *Cavendish Laboratory, Department of Physics and Department of Chemical Engineering and Biotechnology, University of Cambridge, Cambridge CB3 0HE, U.K.*

**Krzysztof Gałkowski** − *Cavendish Laboratory, Department of Physics, University of Cambridge, Cambridge CB3 0HE, U.K.; Institute of Physics, Faculty of Physics, Astronomy and Informatics, Nicolaus Copernicus University, Toruń 87−100, Poland;* ⓘ orcid.org/0000-0002-9275-1519

Complete contact information is available at:
https://pubs.acs.org/10.1021/acs.chemmater.0c01255

### Author Contributions

▽D.J.K. and M.S. contributed equally to this work.

### Notes

The authors declare no competing financial interest.

## ■ ACKNOWLEDGMENTS

## ■ REFERENCES

(1) Kojima, A.; Teshima, K.; Shirai, Y.; Miyasaka, T. Organometal Halide Perovskites as Visible-Light Sensitizers for Photovoltaic Cells. *J. Am. Chem. Soc.* **2009**, *131*, 6050−6051.

(2) National Renewable Energy Lab. Renewable Energy Labs Efficiency Chart. http://www.nrel.gov/ncpv/images/efficiency_chart.jpg 2020, Accessed February 19 2020.

(3) Yang, W. S.; Park, B.-W.; Jung, E. H.; Jeon, N. J.; Kim, Y. C.; Lee, D. U.; Shin, S. S.; Seo, J.; Kim, E. K.; Noh, J. H.; Seok, S. I. Iodide Management in Formamidinium-Lead-Halide−Based Perovskite Layers for Efficient Solar Cells. *Science* **2017**, *356*, 1376−1379.

(4) Lyu, M.; Yun, J.-H.; Chen, P.; Hao, M.; Wang, L. Addressing Toxicity of Lead: Progress and Applications of Low-Toxic Metal Halide Perovskites and Their Derivatives. *Adv. Energy Mater.* **2017**, *7*, 1602512.

(5) Hao, F.; Stoumpos, C. C.; Cao, D. H.; Chang, R. P. H.; Kanatzidis, M. G. Lead-Free Solid-State Organic-Inorganic Halide Perovskite Solar Cells. *Nat. Photonics* **2014**, *8*, 489−494.

(6) Noel, N. K.; Stranks, S. D.; Abate, A.; Wehrenfennig, C.; Guarnera, S.; Haghighirad, A.-A.; Sadhanala, A.; Eperon, G. E.; Pathak, S. K.; Johnston, M. B.; Petrozza, A.; Herz, L. M.; Snaith, H. J. Lead-Free Organic-Inorganic Tin Halide Perovskites for Photovoltaic Applications. *Energy Environ. Sci.* **2014**, *7*, 3061−3068.

(7) Liang, L.; Gao, P. Lead-Free Hybrid Perovskite Absorbers for Viable Application: Can We Eat the Cake and Have It Too? *Adv. Sci.* **2018**, *5*, 1700331.

(8) Stoumpos, C. C.; Malliakas, C. D.; Kanatzidis, M. G. Semiconducting Tin and Lead Iodide Perovskites with Organic Cations: Phase Transitions, High Mobilities, and near-Infrared Photoluminescent Properties. *Inorg. Chem.* **2013**, *52*, 9019−9038.

(9) Slavney, A. H.; Leppert, L.; Valdes, A. S.; Bartesaghi, D.; Savenije, T. J.; Neaton, J. B.; Karunadasa, H. I. Small-Band-Gap Halide Double Perovskites. *Angew. Chem., Int. Ed.* **2018**, *57*, 12765−12770.

(10) Zhou, J.; Xia, Z.; Molokeev, M. S.; Zhang, X.; Peng, D.; Liu, Q. Composition Design, Optical Gap and Stability Investigations of Lead-Free Halide Double Perovskite Cs2AgInCl6. *J. Mater. Chem. A* **2017**, *5*, 15031−15037.

(11) Luo, J.; Li, S.; Wu, H.; Zhou, Y.; Li, Y.; Liu, J.; Li, J.; Li, K.; Yi, F.; Niu, G.; Tang, J. Cs2AgInCl6 Double Perovskite Single Crystals: Parity Forbidden Transitions and Their Application For Sensitive and Fast UV Photodetectors. *ACS Photonics* **2018**, *5*, 398−405.

(12) Volonakis, G.; Haghighirad, A. A.; Milot, R. L.; Sio, W. H.; Filip, M. R.; Wenger, B.; Johnston, M. B.; Herz, L. M.; Snaith, H. J.; Giustino, F. Cs2InAgCl6: A New Lead-Free Halide Double Perovskite with Direct Band Gap. *J. Phys. Chem. Lett.* **2017**, *8*, 772−778.

(13) Du, K.; Meng, W.; Wang, X.; Yan, Y.; Mitzi, D. B. Bandgap Engineering of Lead-Free Double Perovskite Cs2AgBiBr6 through Trivalent Metal Alloying. *Angew. Chem., Int. Ed.* **2017**, *56*, 8158−8162.

(14) Vargas, B.; Ramos, E.; Pérez-Gutiérrez, E.; Alonso, J. C.; Solis-Ibarra, D. A Direct Bandgap Copper-Antimony Halide Perovskite. *J. Am. Chem. Soc.* **2017**, *139*, 9116−9119.

(15) Li, X.; Zhong, X.; Hu, Y.; Li, B.; Sheng, Y.; Zhang, Y.; Weng, C.; Feng, M.; Han, H.; Wang, J. Organic-Inorganic Copper(II)-Based Material: A Low-Toxic, Highly Stable Light Absorber for Photovoltaic Application. *J. Phys. Chem. Lett.* **2017**, *8*, 1804−1809.

(16) McClure, E. T.; Ball, M. R.; Windl, W.; Woodward, P. M. Cs2AgBiX6 (X = Br, Cl): New Visible Light Absorbing, Lead-Free Halide Perovskite Semiconductors. *Chem. Mater.* **2016**, *28*, 1348−1354.

(17) Slavney, A. H.; Hu, T.; Lindenberg, A. M.; Karunadasa, H. I. A Bismuth-Halide Double Perovskite with Long Carrier Recombination Lifetime for Photovoltaic Applications. *J. Am. Chem. Soc.* **2016**, *138*, 2138−2141.

(18) Filip, M. R.; Hillman, S.; Haghighirad, A. A.; Snaith, H. J.; Giustino, F. Band Gaps of the Lead-Free Halide Double Perovskites Cs2BiAgCl6 and Cs2BiAgBr6 from Theory and Experiment. *J. Phys. Chem. Lett.* **2016**, *7*, 2579−2585.

(19) Igbari, F.; Wang, R.; Wang, Z.-K.; Ma, X.-J.; Wang, Q.; Wang, K.-L.; Zhang, Y.; Liao, L.-S.; Yang, Y. Composition Stoichiometry of Cs2AgBiBr6 Films for Highly Efficient Lead-Free Perovskite Solar Cells. *Nano Lett.* **2019**, *19*, 2066−2073.

(20) Greul, E.; Petrus, M. L.; Binek, A.; Docampo, P.; Bein, T. Highly Stable, Phase Pure Cs2AgBiBr6 Double Perovskite Thin Films for Optoelectronic Applications. *J. Mater. Chem. A* **2017**, *5*, 19972−19981.

(21) Filip, M. R.; Liu, X.; Miglio, A.; Hautier, G.; Giustino, F. Phase Diagrams and Stability of Lead-Free Halide Double Perovskites Cs2BB′X6: B = Sb and Bi, B′ = Cu, Ag, and Au, and X = Cl, Br, and I. *J. Phys. Chem. C* **2018**, *122*, 158−170.

(22) Lozhkina, O. A.; Murashkina, A. A.; Elizarov, M. S.; Shilovskikh, V. V.; Zolotarev, A. A.; Kapitonov, Y. V.; Kevorkyants, R.; Emeline, A. V.; Miyasaka, T. Microstructural Analysis and Optical Properties of the Halide Double Perovskite Cs2BiAgBr6 Single Crystals. *Chem. Phys. Lett.* **2018**, *694*, 18−22.

(23) Schade, L.; Wright, A. D.; Johnson, R. D.; Dollmann, M.; Wenger, B.; Nayak, P. K.; Prabhakaran, D.; Herz, L. M.; Nicholas, R.; Snaith, H. J.; Radaelli, P. G. Structural and Optical Properties of Cs2AgBiBr6 Double Perovskite. *ACS Energy Lett.* **2019**, *4*, 299−305.

(24) Du, K.; Wang, X.; Han, Q.; Yan, Y.; Mitzi, D. B. Heterovalent B-Site Co-Alloying Approach for Halide Perovskite Bandgap Engineering. *ACS Energy Lett.* **2017**, *2*, 2486−2490.

(25) Lindquist, K. P.; Mack, S. A.; Slavney, A. H.; Leppert, L.; Gold-Parker, A.; Stebbins, J. F.; Salleo, A.; Toney, M. F.; Neaton, J. B.; Karunadasa, H. I. Tuning the Bandgap of Cs2AgBiBr6 through Dilute Tin Alloying. *Chem. Sci.* **2019**, *10*, 10620−10628.

(26) Su, J.; Mou, T.; Wen, J.; Wang, B. First-Principles Study on the Structure, Electronic, and Optical Properties of Cs2AgBiBr6-XClx Mixed-Halide Double Perovskites. *J. Phys. Chem. C* **2020**, *124*, 5371−5377.

(27) Kumar Chini, M.; Goverapet Srinivasan, S.; Tailor, N. K.; Yukta; Salahub, D.; Satapathi, S. Lead-Free, Stable Mixed Halide Double Perovskites Cs2AgBiBr6 and Cs2AgBiBr6−xClx − A Detailed Theoretical and Experimental Study. *Chem. Phys.* **2020**, *529*, 110547.

(28) Gray, M. B.; McClure, E. T.; Woodward, P. M. Cs2AgBiBr6−xClx Solid Solutions−Band Gap Engineering with Halide Double Perovskites. *J. Mater. Chem. C* **2019**, *7*, 9686−9689.

(29) Rosales, B. A.; Men, L.; Cady, S. D.; Hanrahan, M. P.; Rossini, A. J.; Vela, J. Persistent Dopants and Phase Segregation in Organolead Mixed-Halide Perovskites. *Chem. Mater.* **2016**, *28*, 6848−6859.

(30) Franssen, W. M. J.; Kentgens, A. P. M. Solid−State NMR of Hybrid Halide Perovskites. *Solid State Nucl. Magn. Reson.* **2019**, *100*, 36−44.

(31) Kubicki, D. J.; Prochowicz, D.; Hofstetter, A.; Péchy, P.; Zakeeruddin, S. M.; Grätzel, M.; Emsley, L. Cation Dynamics in Mixed-Cation (MA)x(FA)1-XPbI3 Hybrid Perovskites from Solid-State NMR. *J. Am. Chem. Soc.* **2017**, *139*, 10055−10061.

(32) Kubicki, D. J.; Prochowicz, D.; Hofstetter, A.; Zakeeruddin, S. M.; Grätzel, M.; Emsley, L. Phase Segregation in Cs-, Rb- and K-Doped Mixed-Cation (MA)x(FA)1−XPbI3 Hybrid Perovskites from Solid-State NMR. *J. Am. Chem. Soc.* **2017**, *139*, 14173−14180.

(33) Kubicki, D. J.; Prochowicz, D.; Hofstetter, A.; Zakeeruddin, S. M.; Grätzel, M.; Emsley, L. Phase Segregation in Potassium-Doped Lead Halide Perovskites from 39K Solid-State NMR at 21.1 T. *J. Am. Chem. Soc.* **2018**, *140*, 7232−7238.

(34) Kubicki, D. J.; Prochowicz, D.; Hofstetter, A.; Saski, M.; Yadav, P.; Bi, D.; Pellet, N.; Lewiński, J.; Zakeeruddin, S. M.; Grätzel, M.; Emsley, L. Formation of Stable Mixed Guanidinium−Methylammonium Phases with Exceptionally Long Carrier Lifetimes for High-Efficiency Lead Iodide-Based Perovskite Photovoltaics. *J. Am. Chem. Soc.* **2018**, *140*, 3345−3351.

(35) Kubicki, D. J.; Prochowicz, D.; Pinon, A.; Stevanato, G.; Hofstetter, A.; Zakeeruddin, S. M.; Grätzel, M.; Emsley, L. Doping and Phase Segregation in Mn2+− and Co2+−Doped Lead Halide Perovskites from 133Cs and 1H NMR Relaxation Enhancement. *J. Mater. Chem. A* **2019**, *7*, 2326−2333.

(36) Karmakar, A.; Dodd, M. S.; Agnihotri, S.; Ravera, E.; Michaelis, V. K. Cu(II)-Doped Cs2SbAgCl6 Double Perovskite: A Lead-Free, Low-Bandgap Material. *Chem. Mater.* **2018**, *30*, 8280−8290.

(37) Franssen, W. M. J.; Bruijnaers, B. J.; Portengen, V. H. L.; Kentgens, A. P. M. Dimethylammonium Incorporation in Lead Acetate Based MAPbI3 Perovskite Solar Cells. *ChemPhysChem* **2018**, *19*, 3107−3115.

(38) Xiang, W.; Wang, Z.; Kubicki, D. J.; Wang, X.; Tress, W.; Luo, J.; Zhang, J.; Hofstetter, A.; Zhang, L.; Emsley, L.; Grätzel, M.; Hagfeldt, A. Ba-Induced Phase Segregation and Band Gap Reduction in Mixed-Halide Inorganic Perovskite Solar Cells. *Nat. Commun.* **2019**, *10*, 1−8.

(39) Xiang, W.; Wang, Z.; Kubicki, D. J.; Tress, W.; Luo, J.; Prochowicz, D.; Akin, S.; Emsley, L.; Zhou, J.; Dietler, G.; Grätzel, M.; Hagfeldt, A. Europium-Doped CsPbI 2 Br for Stable and Highly Efficient Inorganic Perovskite Solar Cells. *Joule* **2019**, *3*, 205−214.

(40) Hanrahan, M. P.; Men, L.; Rosales, B. A.; Vela, J.; Rossini, A. J. Sensitivity-Enhanced 207Pb Solid-State NMR Spectroscopy for the Rapid, Non-Destructive Characterization of Organolead Halide Perovskites. *Chem. Mater.* **2018**, *30*, 7005−7015.

(41) Rosales, B. A.; Hanrahan, M. P.; Boote, B. W.; Rossini, A. J.; Smith, E. A.; Vela, J. Lead Halide Perovskites: Challenges and Opportunities in Advanced Synthesis and Spectroscopy. *ACS Energy Lett.* **2017**, *2*, 906−914.

(42) Karmakar, A.; Askar, A. M.; Bernard, G. M.; Terskikh, V. V.; Ha, M.; Patel, S.; Shankar, K.; Michaelis, V. K. Mechanochemical Synthesis of Methylammonium Lead Mixed−Halide Perovskites: Unraveling the Solid-Solution Behavior Using Solid-State NMR. *Chem. Mater.* **2018**, *30*, 2309−2321.

(43) Askar, A. M.; Karmakar, A.; Bernard, G. M.; Ha, M.; Terskikh, V. V.; Wiltshire, B. D.; Patel, S.; Fleet, J.; Shankar, K.; Michaelis, V. K. Composition-Tunable Formamidinium Lead Mixed Halide Perovskites via Solvent-Free Mechanochemical Synthesis: Decoding the Pb Environments Using Solid-State NMR Spectroscopy. *J. Phys. Chem. Lett.* **2018**, *9*, 2671−2677.

(44) Karmakar, A.; Dodd, M. S.; Zhang, X.; Oakley, M. S.; Klobukowski, M.; Michaelis, V. K. Mechanochemical Synthesis of 0D and 3D Cesium Lead Mixed Halide Perovskites. *Chem. Commun.* **2019**, *55*, 5079−5082.

(45) Bi, D.; Li, X.; Milić, J. V.; Kubicki, D. J.; Pellet, N.; Luo, J.; LaGrange, T.; Mettraux, P.; Emsley, L.; Zakeeruddin, S. M.; Grätzel, M. Multifunctional Molecular Modulators for Perovskite Solar Cells with over 20% Efficiency and High Operational Stability. *Nat. Commun.* **2018**, *9*, 4482.

(46) Alharbi, E. A.; Alyamani, A. Y.; Kubicki, D. J.; Uhl, A. R.; Walder, B. J.; Alanazi, A. Q.; Luo, J.; Burgos-Caminal, A.; Albadri, A.; Albrithen, H.; Alotaibi, M. H.; Moser, J.-E.; Zakeeruddin, S. M.; Giordano, F.; Emsley, L.; Grätzel, M. Atomic-Level Passivation Mechanism of Ammonium Salts Enabling Highly Efficient Perovskite Solar Cells. *Nat. Commun.* **2019**, *10*, 1−9.

(47) Alanazi, A. Q.; Kubicki, D. J.; Prochowicz, D.; Alharbi, E. A.; Bouduban, M. E.; Jahanbakhshi, F.; Mladenović, M.; Milić, J. V.; Giordano, F.; Ren, D. Atomic-Level Microstructure of Efficient Formamidinium-Based Perovskite Solar Cells Stabilized by 5-Ammonium Valeric Acid Iodide Revealed by Multinuclear and Two-Dimensional Solid-State NMR. *J. Am. Chem. Soc.* **2019**, *141*, 17659−17669.

(48) Tavakoli, M. M.; Tress, W.; Milić, J. V.; Kubicki, D.; Emsley, L.; Grätzel, M. Addition of Adamantylammonium Iodide to Hole Transport Layers Enables Highly Efficient and Electroluminescent Perovskite Solar Cells. *Energy Environ. Sci.* **2018**, *11*, 3310−3320.

(49) Askar, A. M.; Bernard, G. M.; Wiltshire, B.; Shankar, K.; Michaelis, V. K. Multinuclear Magnetic Resonance Tracking of Hydro, Thermal, and Hydrothermal Decomposition of CH3NH3PbI3. *J. Phys. Chem. C* **2017**, *121*, 1013−1024.

(50) Wasylishen, R. E.; Knop, O.; MacDonald, J. B. Cation Rotation in Methylammonium Lead Halides. *Solid State Commun.* **1985**, *56*, 581−582.

(51) Knop, O.; Wasylishen, R. E.; White, M. A.; Cameron, T. S.; Van Oort, M. J. M. Alkylammonium Lead Halides. Part 2. CH3NH3PbX3 (X = Chlorine, Bromine, Iodine) Perovskites: Cuboctahedral Halide Cages with Isotropic Cation Reorientation. *Can. J. Chem.* **1990**, *68*, 412−422.

(52) Franssen, W. M. J.; Van Es, S. G. D.; Dervişoğlu, R.; De Wijs, G. A.; Kentgens, A. P. M. Symmetry, Dynamics, and Defects in Methylammonium Lead Halide Perovskites. *J. Phys. Chem. Lett.* **2017**, *8*, 61−66.

(53) Bernard, G. M.; Wasylishen, R. E.; Ratcliffe, C. I.; Terskikh, V.; Wu, Q.; Buriak, J. M.; Hauger, T. Methylammonium Cation Dynamics in Methylammonium Lead Halide Perovskites: A Solid-State NMR Perspective. *J. Phys. Chem. A* **2018**, *122*, 1560−1573.

(54) Senocrate, A.; Moudrakovski, I.; Kim, G. Y.; Yang, T.-Y.; Gregori, G.; Grätzel, M.; Maier, J. The Nature of Ion Conduction in Methylammonium Lead Iodide: A Multimethod Approach. *Angew. Chem., Int. Ed.* **2017**, *56*, 7755−7759.

(55) Senocrate, A.; Moudrakovski, I.; Maier, J. Short-Range Ion Dynamics in Methylammonium Lead Iodide by Multinuclear Solid State NMR and 127I NQR. *Phys. Chem. Chem. Phys.* **2018**, *20*, 20043−20055.

(56) Senocrate, A.; Moudrakovski, I.; Acartürk, T.; Merkle, R.; Kim, G. Y.; Starke, U.; Grätzel, M.; Maier, J. Slow CH3NH3+ Diffusion in CH3NH3PbI3 under Light Measured by Solid-State NMR and Tracer Diffusion. *J. Phys. Chem. C* **2018**, *122*, 21803−21806.

(57) Harris, R. K.; Becker, E. D.; Cabral de Menezes, S. M.; Goodfellow, R.; Granger, P. NMR Nomenclature: Nuclear Spin Properties and Conventions for Chemical Shifts: IUPAC Recommendations 2001. *Solid State Nucl. Magn. Reson.* **2002**, *22*, 458−483.

(58) Prochowicz, D.; Yadav, P.; Saliba, M.; Kubicki, D. J.; Tavakoli, M. M.; Zakeeruddin, S. M.; Lewiński, J.; Emsley, L.; Grätzel, M. One-Step Mechanochemical Incorporation of an Insoluble Cesium Additive for High Performance Planar Heterojunction Solar Cells. *Nano Energy* **2018**, *49*, 523−528.

(59) Skibsted, J.; Vosegaard, T.; Bildsøe, H.; Jakobsen, H. J. 133Cs Chemical Shielding Anisotropies and Quadrupole Couplings from Magic-Angle Spinning NMR of Cesium Salts. *J. Phys. Chem.* **1996**, *100*, 14872−14881.

(60) Whittle, K. R.; Lumpkin, G. R.; Ashbrook, S. E. Neutron Diffraction and MAS NMR of Cesium Tungstate Defect Pyrochlores. *J. Solid State Chem.* **2006**, *179*, 512−521.

(61) Michaelis, V. K.; Aguiar, P. M.; Kroeker, S. Probing Alkali Coordination Environments in Alkali Borate Glasses by Multinuclear Magnetic Resonance. *J. Non-Cryst. Solids* **2007**, *353*, 2582−2590.

(62) Reinhold, C. J.; Anderson, P. A.; Edwards, P. P.; Terskikh, V. V.; Ratcliffe, C. I.; Ripmeester, J. A. 133Cs NMR and ESR Studies of Cesium-Loaded LiX and LiA Zeolites. *J. Phys. Chem. C* **2008**, *112*, 17796−17803.

(63) Kim, Y.; James Kirkpatrick, R.; Cygan, R. T. 133Cs NMR Study of Cesium on the Surfaces of Kaolinite and Illite. *Geochim. Cosmochim. Acta* **1996**, *60*, 4059−4074.

(64) Simović, B.; Jérome, D.; Rachdi, F.; Baumgartner, G.; Forró, L. 133Cs and 13C-NMR in CsC60 Polymers under Pressure. *Synth. Met.* **1999**, *103*, 2399−2402.

(65) Hughes, E.; Jordan, J.; Gullion, T. Structural Characterization of the [Cs(p-Tert-Butylcalix[4]Arene −H)(MeCN)] Guest−Host System by 13C-133Cs REDOR NMR. *J. Phys. Chem. B* **2001**, *105*, 5887−5891.

(66) Do, J.-L.; Friščić, T. Mechanochemistry: A Force of Synthesis. *ACS Cent. Sci.* **2017**, *3*, 13−19.

(67) Prochowicz, D.; Saski, M.; Yadav, P.; Grätzel, M.; Lewiński, J. Mechanoperovskites for Photovoltaic Applications: Preparation, Characterization, and Device Fabrication. *Acc. Chem. Res.* **2019**, *52*, 3233−3243.

(68) Prochowicz, D.; Franckevičius, M.; Cieślak, A. M.; Zakeeruddin, S. M.; Grätzel, M.; Lewiński, J. Mechanosynthesis of the Hybrid Perovskite CH3NH3PbI3: Characterization and the Corresponding Solar Cell Efficiency. *J. Mater. Chem. A* **2015**, *3*, 20772−20777.

(69) Prochowicz, D.; Yadav, P.; Saliba, M.; Saski, M.; Zakeeruddin, S. M.; Lewiński, J.; Grätzel, M. Mechanosynthesis of Pure Phase Mixed-Cation MAxFA1-XPbI3 Hybrid Perovskites: Photovoltaic Performance and Electrochemical Properties. *Sustain. Energy Fuels* **2017**, *1*, 689−693.

(70) Saski, M.; Prochowicz, D.; Marynowski, W.; Lewiński, J. Mechanosynthesis, Optical, and Morphological Properties of MA, FA, Cs-SnX3 (X = I, Br) and Phase-Pure Mixed-Halide MASnIxBr3−x Perovskites. *Eur. J. Inorg. Chem.* **2019**, *2019*, 2680−2684.

(71) de Mello, J. C.; Wittmann, H. F.; Friend, R. H. An Improved Experimental Determination of External Photoluminescence Quantum Efficiency. *Adv. Mater.* **1997**, *9*, 230−232.

(72) Rosales, B. A.; Wei, L.; Vela, J. Synthesis and Mixing of Complex Halide Perovskites by Solvent-Free Solid-State Methods. *J. Solid State Chem.* **2019**, *271*, 206−215.

(73) García-Espejo, G.; Rodríguez-Padrón, D.; Luque, R.; Camacho, L.; Miguel, G. d. Mechanochemical Synthesis of Three Double Perovskites: Cs2AgBiBr6, (CH3NH3)2TlBiBr6 and Cs2AgSbBr6. *Nanoscale* **2019**, *11*, 16650−16657.

(74) Ashbrook, S. E.; Whittle, K. R.; Lumpkin, G. R.; Farnan, I. 89Y Magic-Angle Spinning NMR of Y2Ti2-XSnxO7 Pyrochlores. *J. Phys. Chem. B* **2006**, *110*, 10358−10364.

(75) Moran, R. F.; McKay, D.; Tornstrom, P. C.; Aziz, A.; Fernandes, A.; Grau-Crespo, R.; Ashbrook, S. E. Ensemble-Based Modeling of the NMR Spectra of Solid Solutions: Cation Disorder in Y2(Sn,Ti)2O7. *J. Am. Chem. Soc.* **2019**, *141*, 17838−17846.

(76) Kubicki, D. J.; Prochowicz, D.; Salager, E.; Rakhmatullin, A.; Grey, C. P.; Emsley, L.; Stranks, S. D. Local Structure and Dynamics in Methylammonium, Formamidinium, and Cesium Tin(II) Mixed-Halide Perovskites from 119Sn Solid-State NMR. *J. Am. Chem. Soc.* **2020**, *142*, 7813−7826.

(77) Hamdeh, U. H.; Nelson, R. D.; Ryan, B. J.; Bhattacharjee, U.; Petrich, J. W.; Panthani, M. G. Solution-Processed All-Inorganic Bismuth-Triiodide Thin-Films for Photovoltaic Application. *Chem. Mater.* **2017**, *28*, 6567−6574.

(78) Creutz, S. E.; Crites, E. N.; De Siena, M. C.; Gamelin, D. R. Colloidal Nanocrystals of Lead-Free Double-Perovskite (Elpasolite) Semiconductors: Synthesis and Anion Exchange To Access New Materials. *Nano Lett.* **2018**, *18*, 1118−1123.

(79) Ivanov, Y. N.; Sukhovskii, A. A.; Lisin, V. V.; Aleksandrova, I. P. Phase Transitions of Cs3Sb2I9 , Cs3Bi2I9 , and Cs3Bi2Br9 Crystals. *Inorg. Mater.* **2001**, *37*, 623−627.

(80) Hoye, R. L. Z.; Eyre, L.; Wei, F.; Brivio, F.; Sadhanala, A.; Sun, S.; Li, W.; Zhang, K. H. L.; MacManus-Driscoll, J. L.; Bristowe, P. D.; Friend, R. H.; Cheetham, A. K.; Deschler, F. Fundamental Carrier Lifetime Exceeding 1 Ms in Cs2 AgBiBr6 Double Perovskite. *Adv. Mater. Interfaces* **2018**, *5*, 1800464.

(81) Li, S.; Luo, J.; Liu, J.; Tang, J. Self-Trapped Excitons in All-Inorganic Halide Perovskites: Fundamentals, Status, and Potential Applications. *J. Phys. Chem. Lett.* **2019**, *10*, 1999−2007.

(82) Ke, B.; Zeng, R.; Zhao, Z.; Wei, Q.; Xue, X.; Bai, K.; Cai, C.; Zhou, W.; Xia, Z.; Zou, B. Homo- and Heterovalent Doping-Mediated Self-Trapped Exciton Emission and Energy Transfer in Mn-Doped Cs2Na1−XAgxBiCl6 Double Perovskites. *J. Phys. Chem. Lett.* **2020**, *11*, 340−348.

(83) McCall, K. M.; Stoumpos, C. C.; Kostina, S. S.; Kanatzidis, M. G.; Wessels, B. W. Strong Electron-Phonon Coupling and Self-

Trapped Excitons in the Defect Halide Perovskites A3M2I9 (A = Cs, Rb; M = Bi, Sb). *Chem. Mater.* **2017**, *29*, 4129−4145.

(84) deQuilettes, D. W.; Frohna, K.; Emin, D.; Kirchartz, T.; Bulovic, V.; Ginger, D. S.; Stranks, S. D. Charge-Carrier Recombination in Halide Perovskites. *Chem. Rev.* **2019**, *119*, 11007−11019.

(85) Zelewski, S. J.; Urban, J. M.; Surrente, A.; Maude, D. K.; Kuc, A.; Schade, L.; Johnson, R. D.; Dollmann, M.; Nayak, P. K.; Snaith, H. J.; Radaelli, P.; Kudrawiec, R.; Nicholas, R. J.; Plochocka, P.; Baranowski, M. Revealing the Nature of Photoluminescence Emission in the Metal-Halide Double Perovskite Cs2AgBiBr6. *J. Mater. Chem. C* **2019**, *7*, 8350−8356.